Scripta METALLURGICA et MATERIALIA
Vol. 25, pp. 2497-2502, 1991
Printed in the U.S.A.
Pergamon Press plc

The Effects of Segregation on Grain Boundary Cohesive Energies in $Ni_{3-x}Al_{1+x}$

R. Najafabadi†, H.Y. Wang†, D. J. Srolovitz†, R. LeSar*
†Department of Materials Science and Engineering, University of Michigan
Ann Arbor, MI 48109, USA
*Theoretical Division, Los Alamos National Laboratory
Los Alamos, NM 87545, USA

(Received June 5, 1991)
(Revised August 27, 1991)

Introduction

The structure and properties of grain boundaries in the intermetallic alloy Ni3Al have received considerable attention in the past several years due to their interesting mechanical properties. The aim in many of these studies [1-13] was to explain the increase in ductility that occurs when polycrystalline Ni3Al is doped with boron. Experimental observations [1-7] have shown that there is a strong correlation between nickel enrichment at grain boundaries and the ductilization of boron-doped polycrystalline Ni3Al. This grain boundary nickel enrichment has only been observed in Ni-rich $Ni_{3-x}Al_{1+x}$ (i.e., $x<0$). Some experimental studies have shown that grain boundary nickel enrichment also occurs in Ni-rich, boron-free polycrystalline $Ni_{3-x}Al_{1+x}$ [3,7]. Two models have been proposed [14,15] to explain the observed ductilization of polycrstalline Ni3Al. In the first model [e.g. 14], an increase in grain boundary cohesive energy has been attributed to nickel enrichment at the grain boundaries, while in the other model [15], it is suggested that the transmittal of slip across the grain boundary becomes easier in chemically disordered grain boundaries, where the disorder is induced by the nickel enrichment at grain boundaries. While these two purported effects of nickel segregation are not necessarily exclusive, experimental studies have been unable to conclusively validate either.

There have been several atomistic simulation studies [8-13] that have been carried out to explore this subject. Most of these simulation studies [8-11] have been done at zero temperature and without direct consideration of the important segregation effects. These studies have shown that the cohesive energy for grain boundaries rich in nickel is lower than that for the same boundaries with aluminum-rich or stoichiometric compositions. One of these same studies [9] has shown that the grain boundary cohesive energy can be reduced even further by placing boron atoms in interstitial sites in the boundary. These results seem to give some credibility to the first model, since these changes in the cohesive energy occur for boundaries that are well ordered. One should note, however, that these simulations are carried out with stoichiometric bulk compositions, not at the nickel rich bulk compositions, where nickel enrichment of the grain boundaries and ductilization are experimentally observed. Due to the nature of the zero-temperature, fixed composition simulation method used in these studies, it was not possible to study the variation in grain boundary cohesive energy that occurs with segregation and equilibrium disordering. Monte Carlo simulation studies [12] at 1000 K have shown that grain boundaries become enriched with nickel and aluminum for Ni-rich and Al-rich bulk composition, respectively.

In this letter, we report the results of our investigations of segregation effects on grain boundary cohesive energy in ordered, boron-free $Ni_{3-x}Al_{1+x}$ within the framework of an atomistic simulation procedure. Segregation to two high angle (001) twist grain boundaries $\Sigma5$ (36.9°) and $\Sigma13$ (22.6°) and to (001) free surfaces are studied using a newly developed, free energy minimization method [16-18]. These simulations are carried out for a range of alloy compositions corresponding to nickel concentrations in the bulk of 73.5, 75.0, and 76.6 atomic percent in the temperature range 300-900 K. This model is also used to investigate the degree of chemical disordering that occurs at the grain boundaries. The two existing models for the role of Ni segregation on the ductilization of Ni3Al are discussed in light of the present simulation results.

Method

The local harmonic (LH) model has been applied with considerable success to both perfect and defected single component solids [16,17]. In this model, the classical vibrational contribution to the free energy for a single component system is given by

0036-9748/91 $3.00 + .00

$$A_v = k_B T \sum_{i=1}^{N} \sum_{\beta=1}^{3} \ln\left[\frac{h\omega_{i\beta}}{2\pi k_B T}\right] \quad (1)$$

where k_B is Boltzmann's constant, h is Planck's constant, and ω_{i1}, ω_{i2}, and ω_{i3} are the three vibrational frequencies of atom i. These frequencies may be determined by diagonalizing the local 3x3 dynamical matrix of each atom $D_{i\alpha\beta} = (\partial^2 E/\partial x_{i\alpha}\partial x_{i\beta})$, where $x_{i\alpha}$ and $x_{i\beta}$ correspond to atomic displacements of atom i in the α and β directions, respectively.

In order to study binary alloys within the frame work of the LH model, each atom is replaced by an "effective atom" of mass $m_i = x_a(i)m_a + x_b(i)m_b$. Here, $x_a(i)$ is the probability that atomic site i is occupied by an atom of type a and mass m_a and correspondingly $x_b(i) = 1 - x_a(i)$ is the probability that the same atomic site is occupied by an atom of type b. The vibrational contribution to the free energy is determined from the appropriately averaged local dynamical matrix (for details see reference [18]). Consistent with this effective atom picture, we write the configurational entropy within the point approximation as

$$S_c = -k_B \sum_{i=1}^{N} \{x_a(i) \ln[x_a(i)] + x_b(i) \ln[x_b(i)]\} \quad (2)$$

In the simulations described below, we employ a reduced Grand Canonical ensemble, where the total number of atoms remains fixed but the relative amounts of each atomic species varies. The appropriate thermodynamic potential for this type of ensemble is the Grand potential and is given by

$$\Omega = A + \Delta\mu \sum_{i=1}^{N} x_a(i) = E + A_v - TS_c + \Delta\mu \sum_{i=1}^{N} x_a(i) \quad (3)$$

where A is the Helmholtz free energy, E is the potential energy (see below), and $\Delta\mu$ is the difference in chemical potential between atoms of type a and b. Given $\Delta\mu$, the equilibrium concentration at each atomic site and the atomic structure is determined by minimizing Ω with respect to the atomic site concentrations and the coordinates of the atomic sites.

The simulation cell geometry employed in the present study has been described in detail elsewhere [17]. Briefly, the grain boundary is embedded in a perfect crystal at the desired temperature and composition. In the plane of the boundary, a periodic border condition is enforced. Normal to the boundary plane the simulation cell is bounded by two infinite, mobile but rigid blocks of structurally perfect crystals. The extent of the region in which atoms move independently and the atomic site compositions vary (between the two blocks of perfect crystal) is increased during the course of the simulation to a size such that the free energy and other properties of the grain boundary remains unchanged within the predetermined values. Similar simulation cells were used to study free surfaces. The potential energy and dynamical matrices implicit within the grand potential (see Eqs. (1) and (3)) are all determined via interatomic potentials. The interatomic potentials, employed in the present study, are of the embedded atom method (EAM) type, developed by Voter and Chen [19].

Within the framework of the present grand canonical simulations, the cohesive free energies, γ_{coh}, is defined as:

$$\gamma_{coh}(\Delta\mu,T) = \gamma_{S1}(\Delta\mu,T) + \gamma_{S2}(\Delta\mu,T) - \gamma_{gb}(\Delta\mu,T) \quad (4)$$

where

$$\gamma_x(\Delta\mu,T) = [\Omega_x(\Delta\mu,T) - \Omega_p(\Delta\mu,T)]/A_x \quad (5)$$

In the above equation Ω is grand potential energy at temperature T and chemical potential difference $\Delta\mu$ and the subscripts x and p refer to the system with defect (grain boundary, gb, or free surface, S1 or S2) and perfect crystals, respectively. The cohesive free energy is normalized by, A_x, the defect area.

Depending upon the chemical arrangement of the terminating (002) planes of the two crystals meeting at the symmetrical twist boundaries, there are three distinct types of grain boundaries which correspond to different stacking sequence of the (002) planes; namely, $\alpha\beta\alpha\beta \mid \alpha\beta\alpha\beta$, $\beta\alpha\beta\alpha \mid \alpha\beta\alpha\beta$, and $\alpha\beta\alpha\beta \mid \beta\alpha\beta\alpha$ where α and β refer to planes of pure Ni and an ordered arrangement of 50% Ni and 50% Al, respectively. These different types of grain boundaries correspond to the stoichiometric, Ni-rich, and Al-rich composition in the grain boundary region which have been denoted as 50/100, 100/100, and 50/50, respectively in Ref. [8]. In the case of free surfaces, there are only two possible terminations; one terminating with an α–type (002) plane (S2) and the other one with a β-type (002) plane (S1). In the present study, we focus on the properties of the $\alpha\beta\alpha\beta \mid \alpha\beta\alpha\beta$ type grain boundaries as a function of temperature and composition.

In order to isolate the effect of segregation on the properties of grain boundaries and free surfaces from those due merely to structural relaxation, we have performed two types of simulations for each temperature and bulk composition. In the first, the composition of each atomic site remains fixed at a value corresponding to the sublattice composition in the perfect crystal (no segregation or disordering) and the free energy is minimized with respect to the atom positions. In the second, the composition of each site is allowed to vary along with atom positions, in order to reach the true equilibrium state with equilibrium boundary segregation.

Results

The free energy minimization method, described above, was used to calculate the grain boundary cohesive free energies, as defined by Eq. (5), for the $\Sigma5$ and $\Sigma13$ (001) twist grain boundaries in $Ni_{3-x}Al_{1+x}$ ordered alloys for three different bulk compositions, namely 73.5, 75.0, and 76.5 Ni at. %. These compositions are within the stability range of the $L1_2$ Ni_3Al phase as predicted by the free energy minimization method using the present interatomic potentials [19]. The experimental stability range for the Ni_3Al phase, on the other hand, is limited to approximately 74-76 atomic percent. The effect of temperature on grain boundary cohesive free energies was determined by repeating the simulations for several temperatures: 300, 600, and 900 K. A preliminary report of some of the results of the present study may be found in Ref. 20.

The (002) planar average excess nickel concentrations as a function of (002) plane number, n , are shown in Fig. 1 for the $\Sigma5$ and $\Sigma13$ grain boundaries and the two free surfaces for 73.5% Ni bulk composition (Al-rich) at T=300K. The excess nickel concentration, Δx_n, is defined as the difference in nickel concentration in plane n in the system with an interface and its corresponding value in the perfect crystal. The geometrical grain boundary plane was originally between planes 0 and 1. The terminating (002) plane for the S1 free surface, which was initially at approximately 50% nickel, is plane 0 with other planes numbered in a descending order. For the S2 free surface, the planes are numbered in an ascending order, with the terminating (002) plane, initially nearly pure nickel, at n=1. At 300K, surface S1 shows only a very slight (1%) Ni enrichment, while surface S2 shows an aluminum enrichment of 38%. The $\Sigma5$ and $\Sigma13$ boundaries exhibit peak segregations of 18% and 30% aluminum, respectively. While the grain boundary segregation to the n=0 plane is significantly smaller than for the n=1 plane, it is still substantial. On the other hand, the degree of segregation to any of the other planes is quite small. Comparison of results for 300 and 900 K shows that the main effect of raising temperature is to decrease the overall magnitude of the segregation, while leaving the major trends in the segregation unaltered.

In Figure 2, we show the excess nickel concentration profiles for the grain boundaries and free surfaces at 300 K for a bulk composition of 76.6% Ni (Ni-rich). At T=300K, planes 0 and +2 in the $\Sigma5$ boundary which were initially of approximately 50% Ni have been enriched by 4 and 7% Ni, respectively, and planes -1 and +3, which were similar to planes 0 and +2, are only very slightly enriched in Al. When the temperature is increased to 900K, the peak Ni enrichments are greatly reduced, to about 1%. Similar behavior is observed for the $\Sigma13$ boundary. For the free surfaces at 300 K, planes 0 and +2, corresponding to the planes 0 and +2 in the grain boundaries, are enriched by 18 and 2% Ni, respectively. When the temperature is increased to 900 K, these Ni enrichments are reduced to 8 and 1%, respectively. Also, planes -2 and +4 in the free surfaces, corresponding to -2 and +4 planes in the grain boundaries, are slightly enriched in Al.

Simulations performed at the stoichiometric composition for the three temperatures showed no significant segregation of either Al or Ni to the $\Sigma5$ and $\Sigma13$ grain boundaries and to the S1 free surface. The S2 surface, on the other hand, did exhibit a peak excess of Al of approximately 12% at 300K, which is reduced to nearly zero at 900K.

The $\Sigma5$ and $\Sigma13$ grain boundary cohesive energies are shown in Table I for different temperatures and bulk compositions. The cohesive energy, γ^u_{coh}, is calculated using Eq. (5) in the zero segregation limit. The cohesive energy, γ^s_{coh}, is calculated for the case of equilibrium segregation to the grain boundaries and to the free surfaces. The difference between these cohesive energies, $(\gamma^s_{coh} - \gamma^u_{coh})$, for a given temperature and bulk composition shows the degree to which segregation makes the boundaries weaker (negative) or stronger (positive). For both the $\Sigma5$ and $\Sigma13$ grain boundaries, the effect of segregation (for the temperatures studied here) is to slightly weaken the boundaries (< 2%) for both the Ni-rich and Al-rich compositions and is essentially negligible for stoichiometric composition.

The variation in the grain boundary cohesive energy, γ^s_{coh}, as a function of bulk composition is shown in Fig. 3, for the $\Sigma13$ boundary at several different temperatures. For the temperatures studied here, the cohesive energy for the $\Sigma5$ and $\Sigma13$ grain boundaries is smaller for the Al-rich composition than for the stoichiometric composition by about 2 and 4%, respectively. For 300 and 600 K, the cohesive energy is smaller for the Ni-rich composition than for the stoichiometric composition, but become larger at 900K by about 0.5%. In all cases, the cohesive energy decreases with increasing temperature, as shown in Figure 4. The rate of change in the cohesive energy with temperature are similar for the Al-rich and stoichiometric compositions in each of the two boundaries. For the Ni-rich composition, on the other

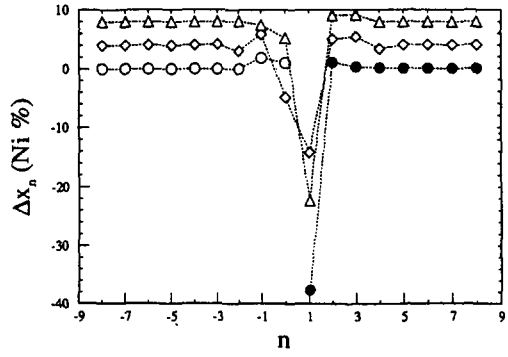

Figure 1. Excess nickel concentration profiles of (002) planes for the $\Sigma 5$ (diamonds) and the $\Sigma 13$ (triangles) boundaries, and the S1(open circles) and the S2 (closed circles) (001) free surfaces for the Al-rich (73.5 %) composition at 300 K($\Sigma 5$ and $\Sigma 13$ results were shifted up by 4 and 8 Ni at %, respectively).

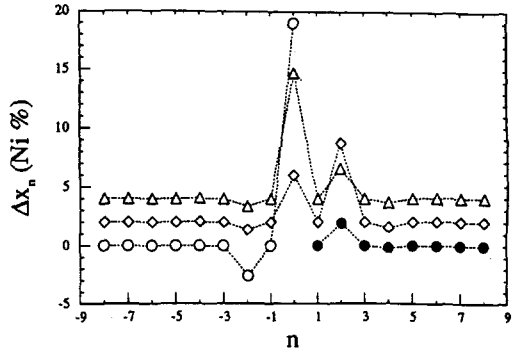

Figure 2. Excess nickel concentration profiles for the Ni-rich composition (76.6 Ni at. %) at 300 K ($\Sigma 5$ and $\Sigma 13$ results were shifted up by 2 and 4 Ni at. %, respectively). Same symbols as in Figure 1.

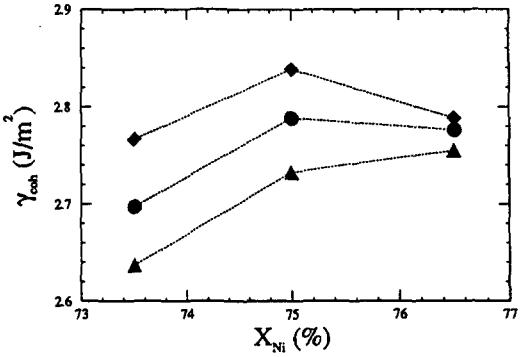

Figure 4. Grain boundary cohesive free energy for the $\Sigma 13$ grain boundary as a function of bulk composition for temperature of 300 (diamonds), 600 (circles), and 900K (triangles).

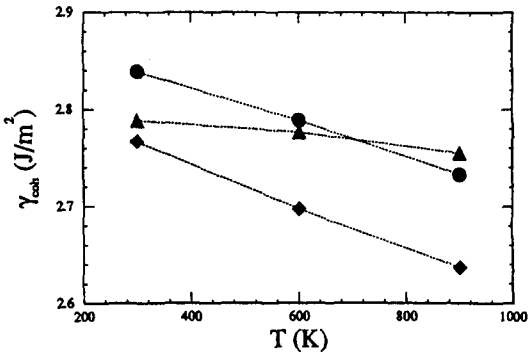

Figure 4. Grain boundary cohesive free energy for the $\Sigma 13$ grain boundary as a function of temperature for Al-rich (diamonds), stiochoimetric(circles), and Ni-rich(triangles) compositions.

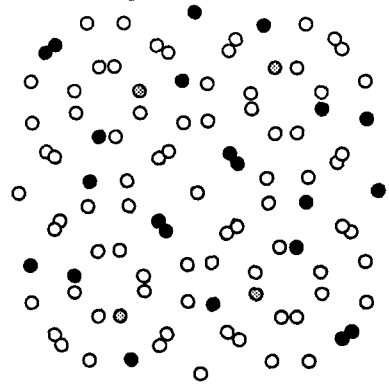

Figure 5. Atomic site concentrations on four (002) planes around the $\Sigma 13$ grain boundary for the Ni-rich composition at 300K. The gray level of the circle indicates composition where black and white correspond to pure Al and Ni, respectively.

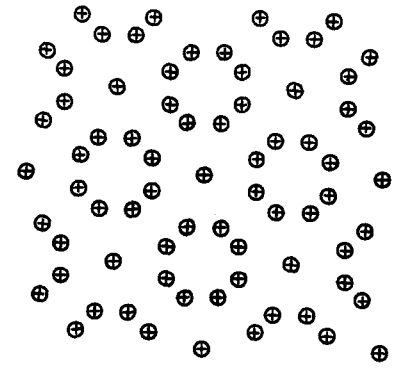

Figure 6. Projection of atoms in four planes around the $\Sigma 5$ grain boundary on to the X-Y plane. Circles represent either Ni or Al atoms and +'s represent Au atoms.

Table I

Calculated grain boundary energy cohesive (in mJ/m^2) for different temperatures and bulk compositions. γ^s_{coh} and γ^u_{coh}, are cohesive energies for the boundaries with and without segregation, respectively. γ^f_{coh} is the difference in the free energy for the grain boundary with segregation and that for the free surfaces with the same composition profile as that of the grain boundary.

		Σ5		Σ13		
T(K)	x (% Ni)	γ^u_{coh}	γ^s_{coh}	γ^u_{coh}	γ^s_{coh}	γ^f_{coh}
300	73.5	2762	2747	2826	2767	2802
	75.0	2776	2774	2840	2839	2839
	76.6	2765	2734	2832	2789	2794
600	73.5	2722	2668	2791	2697	2753
	75.0	2736	2720	2805	2789	2792
	76.6	2726	2705	2798	2776	2794
900	73.5	2686	2608	2763	2637	2715
	75.0	2699	2659	2776	2733	2772
	76.6	2692	2674	2774	2755	2770

hand, the dependence of the cohesive energy on temperature is much more pronounced than for the two other compositions.

Discussion and Conclusions

The cohesive strengths (cohesive energy) of the Σ5 and Σ13 (001) twist grain boundaries in ordered $Ni_{3-x}Al_{1+x}$ for bulk compositions of 73.5, 75.0, and 76.6 % Ni were calculated at different temperatures. Contrary to previous suggestions, it was found that deviations from stoichiometry towards either Ni or Al rich compositions do not improve the strength of the boundaries at 300 and 600 K, but, instead, slightly weakens them. At 900 K, a slight improvement in the grain boundary strength is achieved for both boundaries when the bulk composition becomes Ni-rich. Over the temperature range studied here, there is always nickel or aluminum segregation to the grain boundaries for Ni-rich and Al-rich bulk compositions, respectively. This is consistent with Monte Carlo simulation results [12] carried out at 1000 K.

As a result, the correlation between nickel enrichment at grain boundaries and increases in the cohesive energy, as was previously suggested [14] does not generally hold for these high angle twist boundaries. It has been shown [21] that the plastic work associated with intergranular fracture is strongly dependent on the grain boundary cohesive energy. Therefore, the small improvement in the cohesive energy for the two boundaries at 900 K temperature when bulk composition is Ni-rich might have a significant effect on the fracture behavior in the Ni_3Al model studied. However, this does not account for the improved ductility at lower temperatures, where the opposite trend is obtained.

Examination of nickel site concentrations in the boundaries for the Ni-rich composition shows that the nickel enrichment is limited to only a few (002) planes around the boundaries. Furthermore, the nickel segregation to the boundaries has not induced any significant chemical disordering in the boundary region, see Figure 5, where almost all atomic sites have preserved their perfect crystal preference for Al or Ni atoms. These results are consistent with recent experimental studies [7] on Σ5 twist boundaries in this material which show no disordering up to the boundary plane. As a consequences of these results, one can not, in general, conclude that nickel enrichment induces chemical disordering at grain boundaries. The existence of such chemical disordering is a necessary component of one of the proposed explanations for Ni-segregation induced ductilization of polycrystalline Ni_3Al [15].

It has been shown [11] that the structure of tilt grain boundaries in $L1_2$ binary alloys with strong tendencies toward ordering is quite different than those in single component or solid solution systems. As a result, it has been suggested [11] that the presence of localized regions of excess volume within the boundaries of strongly ordered $L1_2$ materials is partially responsible for intergranular fracture in these materials. In Figure 6, we show the Σ5 (001) twist grain boundary structure in Ni_3Al and in pure gold at 300 K, where the gold lattice constant has been scaled to match that of Ni_3Al. As this figure shows, the two structures are almost indistinguishable. Similar comparisons for the Σ13 boundary also show no real differences between the boundary structures of gold and Ni_3Al. These results show that

there is, at least for the twist boundaries studied here, no significant differences between the boundary structures of $L1_2$ alloys and pure metals.

We recently showed [20] that the grain boundary free energies for these two boundaries in the Al-rich $Ni_{3-x}Al_{1+x}$ decrease by 20% due to aluminum segregation. The same trend, but of smaller magnitude, was observed for the Ni-rich compositions due to nickel segregation to the boundaries. In spite of this fact, the effect of segregation on the grain boundary cohesive energy for all the compositions and temperatures studied here (see Table I) is minimal. This suggests that the decrease in the grain boundary free energy is almost the same as the decreases in the free energies of the two surfaces. This can be better understood by comparing the excess composition profiles for the grain boundaries and the free surfaces as shown in Figs. 2 and 3 for Al-rich and Ni-rich compositions, respectively. The excess concentration profiles perpendicular to the boundary planes for the two grain boundaries are very similar and have the same qualitative behavior as the excess concentration for the two free surfaces.

Recently, it was pointed out [22] that the grain boundary cohesive energy, determined from equilibrium properties of grain boundary and free surfaces as defined by equation 5, does not represent the grain boundary strength in the limit where crack propagation is much faster than the segregation kinetics. In this case, a more reasonable measure of the grain boundary strength, γ^f_{coh}, is the difference in the free energy of the grain boundary at thermodynamic equilibrium and that of the free surfaces with the same concentration profile as the grain boundary [22]. In the last column of Table I we show this cohesive energy for the $\Sigma 13$ grain boundary. γ^f_{coh} always lies between those of the unsegregated and segregated cohesive energies. Comparison of the cohesive energies γ^s_{coh} and γ^f_{coh} for the $\Sigma 13$ boundary shows that the segregation kinetics does not significantly change the grain boundary strength in the Ni_3Al model studied.

In summary, we employed a free energy simulation method to study the cohesive energy of $\Sigma 5$ and $\Sigma 13$ (001) twist grain boundaries in $Ni_{3-x}Al_{1+x}$ as a function of temperature and bulk composition. In the temperature range of 300 to 900K, it is found that the cohesive energy does not significantly change with bulk composition. This constancy of the cohesive energy may be attributed to similar segregation on the grain boundaries and the surfaces formed in intergranular fracture. It is shown that for these high angle, high symmetry (001) symmetrical twist boundaries none of the existing models for the effect of composition on ductility are universally correct. Since the proposals [14,15] that the nickel enrichment of boundaries increases the grain boundary cohesive energy or induces chemical disordering in the boundary region is not valid for these special boundaries, we conclude that these proposals are not generally valid for all grain boundaries.

Acknowledgement - This research was supported by the Division of Materials Science of the Office of Basic Energy Sciences of the U. S. Department of Energy, Grant No. FG02-88ER-45367.

References

1. D. D. Sieloff, S. S. Brenner, and H. Ming Jian, MRS Symp. Proc. **133**, 213 (1989).
2. D. D. Sieloff, S. S. Brenner, and M.G. Burke, MRS Symp. Proc. **83**, 87 (1987).
3. I. Baker, E. M. Schulson, J. R. Michael, and S. J. Pennycook, Phil. Mag. B **62**, 659 (1990).
4. I. Baker, E. M. Schulson, and J. R. Michael, Phil. Mag. B **57**, 379 (1988).
5. E. P. George, C. T. Liu, and R. A. Padgett, Scripta Metall. **23**, 979 (1989).
6. I. Baker and E. M. Schulson, Scripta Metall. **23**, 1883 (1989).
7. H. Kung, D. R. Rasmussen, and S. L. Sass, submitted to Acta Metall. Mater.
8. S. P. Chen, D. J. Srolovitz, and A. F. Voter, J. Mat. Res. **4**, 62 (1989).
9. S. P. Chen, A. F. Voter, R. C. Albers, A. M. Boring, and P. J. Hay, J. Mat. Res. **5**, 955 (1990).
10. G. J. Ackland and V. Vitek, MRS Symp. Proc. **133**, 106 (1989).
11. J. J. Kruisman, V. Vitek, and J. Th. M. De Hosson, Acta Metall. **36**, 2729 (1988).
12. S. M. Foiles and M. S. Daw, J. Mat. Res. **2**, 5 (1987).
13. S. M. Foiles, paper presented at TMS Fall Meeting, Detroit (1990).
14. A. I. Taub and C. L. Briant, Acta Metall. **35**, 427 (1987).
15. E. M. Schulson, I. Baker, and H. J. Frost, MRS Symp. Proc. **83**, 1195 (1987).
16. R. LeSar, R. Najafabadi, and D. J. Srolovitz, Phys. Rev. Lett. **63**, 624 (1989).
17. R. Najafabadi, D. J. Srolovitz, and R. LeSar, J. Mater. Res. **5**, 2663 (1990).
18. R. Najafabadi, H. Y. Wang, D. J. Srolovitz, and R. LeSar, Acta Metall. Mater., in press.
19. A. F. Voter and S. P. Chen, Mat. Res. Soc. Symp. Proc. **82**, 175 (1987).
20. R. Najafabadi, H. Y. Wang, D. J. Srolovitz, and R. LeSar, MRS Symp. Proc. "High Temperature Ordered Intermetallic Alloys", in press (1990).
21. C. J. McMahon and V. Vitek Acta. Metall. **27**, 507 (1979).
22. J. R. Rice and J.-S. Wang, Mat. Sci. and Eng. **A107**, 23 (1989).